

Evolution of a superbubble in a turbulent, multi-phased and magnetized ISM

M.J. Korpi¹, A. Brandenburg², A. Shukurov², and I. Tuominen¹

¹ Department of Physical Sciences, Astronomy Division, University of Oulu, P.O. Box 3000, FIN-90401 Oulu, Finland

² Department of Mathematics, University of Newcastle, Newcastle upon Tyne NE1 7 RU, UK

Received 25 May 1999 / Accepted 15 July 1999

Abstract. The evolution of a superbubble is simulated using a local three-dimensional, non-ideal MHD model, which includes galactic differential rotation, an external gravitational potential, heating via supernova explosions and radiative cooling of the interstellar medium (ISM). In our model a superbubble is formed due to the clustering of supernova activity, mimicking an OB association. Supernovae are modelled as instantaneous explosions that release 10^{51} erg of thermal energy and $3M_{\odot}$ of gas in a small volume. We implement a superbubble with the luminosity 3×10^{37} erg s⁻¹ into an initial ISM, which is taken from our earlier calculations modelling the warm and hot phases of the ISM. The simulated ISM has a multi-phase structure with hot, dilute and warm, denser gas coexisting in pressure equilibrium; there is also some cold, dense gas in the form of clouds and filaments arising from supernova compression. The multicomponent gas is in a state of developed turbulence, with r.m.s. velocity 10 and 40 km s⁻¹ for the warm and hot gas, respectively. At the developed state of the simulation there is a magnetic field of 1.3 μG strength having both uniform and random components.

The evolution of a superbubble is rather different from that indicated by models with quasi-uniform ambient medium. The superbubble loses its spherical symmetry at very early stages of expansion. Its break-through from the disc is strongly facilitated by the nonuniformity of its environment. A superbubble which would be confined in the disc according to criteria obtained for a quasi-uniform ISM can break out to the halo.

Key words: Magnetohydrodynamics (MHD) – turbulence – ISM: general – ISM: structure – ISM: supernova remnants

1. Introduction

There is a vast amount of observational evidence of large (0.1–1 kpc in size) shells of interstellar gas in the Galaxy as well as in other spiral and irregular galaxies from H I 21 cm emission line maps and H II emission line surveys (e.g. McCray & Kafatos 1987; Tenorio-Tagle & Bodenheimer 1988). These superstructures are most likely formed by sequential supernova (hereafter SN) explosions in OB associations (e.g. Tenorio-Tagle & Bo-

denheimer 1988; Spitzer 1990). Clustered SNe create a large, hot, low-density cavity surrounded by a thin, dense shell; such structures are known as superbubbles (hereafter SB). In a typical Galactic OB association, the SN rate is one per 10⁶ yr, maintained approximately constant over 50 Myr (e.g. Heiles 1987; Tenorio-Tagle & Bodenheimer 1988). It has been proposed that a SB can break through the density stratified galactic layer, venting hot gas to the halo through relatively narrow vertical channels known as chimneys (Tomisaka & Ikeuchi 1986, Mac Low & McCray 1988, Norman & Ikeuchi 1989). Structures that can be interpreted as SBs open to the halo have been observed in the Galaxy (e.g. Heiles 1984; Koo et al. 1992; Normandeau et al. 1996).

A variety of models have been developed during recent years to investigate the evolution of SBs. Most of these are two-dimensional hydrodynamic models (e.g. Tomisaka & Ikeuchi 1986; Mac Low & McCray 1988; Mac Low et al. 1989; Tenorio-Tagle et al. 1990), which focussed on conditions for a SB to blow out from the disc under various density stratification profiles. Mac Low & McCray (1988) investigated the expansion of SBs in various stratified disks using the thin shell approximation of Kompaneets. These authors have introduced a dimensionless parameter D that determines whether a SB can break through the gas layer in their model,

$$D = 940 \left(\frac{L}{10^{38} \text{ergs}^{-1}} \right) \left(\frac{n_0}{1 \text{cm}^{-3}} \right)^{1/2} \left(\frac{H}{100 \text{pc}} \right)^{-2} \times \left(\frac{P}{10^4 \text{Kcm}^{-3}} \right)^{-3/2}, \quad (1)$$

where L is the SB mechanical luminosity, n_0 is the ambient number density at the midplane, H is the layer scale height and P is the ambient pressure at the midplane. According to the model of Mac Low & McCray (1988), a SB would break through if $D \gtrsim 100$. Using this criterion, Heiles (1990) concluded that approximately 20 SNe in an OB association ($N_* \approx 20$) are needed for a SB to *break through* the thin Galactic disc containing cold and warm gas components with a Gaussian scale height $H = 190 \text{pc}$ and $n_0 = 0.3 \text{cm}^{-3}$. To *blow out* the extended gas component with $H = 500 \text{pc}$ and $n_0 = 0.1 \text{cm}^{-3}$ (Lockman 1984), $N_* \approx 167$ would be needed. With allowance for the turbulent pressure and the Reynolds (1985, 1991) ionised layer

with $H = 1\text{kpc}$ and $n_0 = 0.025\text{cm}^{-3}$, Koo & McKee (1992) arrived at values $N_* \approx 50$ and $N_* \approx 800$ for the break-through and blow-out, respectively. Since $N_* \approx 50$ in a typical OB association in the Galaxy (e.g. Heiles 1987), SB blow-outs should be rare according to these estimates.

The effect of a uniform magnetic field on the expansion of SBs has been studied e.g. by Ferrière et al. (1991) and Tomisaka (1990, 1998). These authors found that a strong magnetic field can significantly reduce the size of a SB (see also Slavin & Cox 1993). In the three-dimensional MHD model of Tomisaka (1998), a vertically uniform magnetic field of a strength $5\mu\text{G}$ parallel to the galactic disk prevents the blow-out of a SB with $L = 3 \times 10^{37}\text{ergs}^{-1}$ corresponding to $N_* = 50$. This clearly indicates that magnetic effects should be taken into account in criteria similar to Eq. (1). Previous SB models are restricted to a horizontally homogeneous, vertically stratified medium permeated by a uniform magnetic field. Random velocities and magnetic field are neglected.

We consider the evolution of a SB in a strongly nonuniform environment constantly stirred by ongoing SN explosions. The SN activity maintains a realistic multiphase structure of the ISM. We also include magnetic field which, together with the velocity field, has a significant random component. As described in Sect. 2, our model is based on equations of a three-dimensional, non-ideal MHD. The initial state, described in detail in Sect. 3, represents a turbulent, nonuniform ISM at an evolved stage of our earlier simulations (Korpi et al. 1999). We discuss our results in Sect. 4 and present our conclusions in Sect. 5.

2. The model

2.1. Basic equations

We adopt a local Cartesian frame of reference with x , y and z corresponding to the radial, azimuthal and vertical directions, respectively. The centre of the box is moving on a circular orbit with radius R and angular velocity Ω_0 about the Galactic centre. We define a shear parameter $q = -\partial \ln \Omega / \partial \ln r$, where r is the distance from the rotation axis. In our local frame rotational shear translates to a linear shear velocity $u_y^{(0)} = -q\Omega_0 x$ (Wisdom & Tremaine 1988). In the following we solve for the deviations \mathbf{u} from this basic flow. We solve the standard non-ideal MHD equations, namely the induction equation written for the magnetic vector potential, the momentum equation, the energy equation and the continuity equation:

$$\frac{\mathcal{D}\mathbf{A}}{\mathcal{D}t} = \mathbf{u} \times \mathbf{B} + q\Omega_0 A_y \hat{\mathbf{x}} - \eta\mu_0 \mathbf{J}, \quad (2)$$

$$\frac{\mathcal{D}\mathbf{u}}{\mathcal{D}t} = -(\mathbf{u} \cdot \nabla)\mathbf{u} + \mathbf{g} - \frac{1}{\rho}\nabla p + f(\mathbf{u}) + \frac{1}{\rho}\mathbf{J} \times \mathbf{B} + \frac{1}{\rho}\nabla \cdot \boldsymbol{\tau}, \quad (3)$$

$$\frac{\mathcal{D}e}{\mathcal{D}t} = -(\mathbf{u} \cdot \nabla)e - \frac{p}{\rho}(\nabla \cdot \mathbf{u}) + \frac{1}{\rho}\nabla(\chi\rho\nabla e) + 2\nu S^2 + \frac{\eta\mu_0}{\rho}\mathbf{J}^2 + \rho\Lambda + \Gamma, \quad (4)$$

$$\frac{\mathcal{D}\ln \rho}{\mathcal{D}t} = -(\mathbf{u} \cdot \nabla)\ln \rho - \nabla \cdot \mathbf{u} + \Pi, \quad (5)$$

where the total time derivative $\mathcal{D}/\mathcal{D}t = \partial/\partial t + u_y^{(0)}\partial/\partial y$ includes the advection by the basic flow. The following quantities have their usual meaning: $\mathbf{J} = \nabla \times \mathbf{B}/\mu_0$ is the current density, μ_0 the vacuum permeability, η the magnetic diffusivity, χ the thermal diffusivity and $\boldsymbol{\tau} = 2\nu\rho\mathbf{S}$ is the stress tensor, $S_{ij} = \frac{1}{2}(\partial_j u_i + \partial_i u_j - \frac{2}{3}\delta_{ij}\partial_k u_k)$ and ν is the kinematic viscosity. We assume a perfect gas law $p = (\gamma - 1)\rho e$ with $\gamma = c_p/c_v = 5/3$. The temperature is related to internal energy by $e = c_v T$.

In the momentum equation the term $\mathbf{g} = (0, 0, g_z)$ is gravity due to the external gravitational potential. The vertical distribution of the gravitational acceleration has been derived e.g. by Kuijken & Gilmore (1989) and includes contributions from a stellar disk and a spherical halo:

$$g_z = -\frac{a_1 z}{\sqrt{z^2 + z_0^2}} - a_2 z, \quad (6)$$

where $a_1 = 4.4 \times 10^{-9}\text{cms}^{-2}$, $a_2 = 1.7 \times 10^{-9}\text{cms}^{-2}$ and $z_0 = 180\text{pc}$. The term $f(\mathbf{u}) = \Omega_0(2u_y, -(2-q)u_x, 0)$ describes epicyclic deviations from purely circular rotation, which arise from the Coriolis force $\mathbf{F}_C = -2\boldsymbol{\Omega} \times \mathbf{u}$ and part of the inertia force $-u_x du_y^{(0)}/dx = q\Omega_0 u_x$.

SN heating and radiative cooling are introduced as the source and loss terms in the energy equation, Γ and $\rho\Lambda$, respectively. SNe are modelled as instantaneous explosive events releasing thermal energy. The energy is fed into the system via localized heating at a rate (per unit mass)

$$\Gamma = \frac{E_{\text{SN}}}{\rho V \Delta t} \quad (7)$$

where E_{SN} is the explosion energy of a single SN event, ρ is the density at the explosion site, and V is the explosion volume. An explosion occurs during one computational time step, Δt , which is adjusted to be 10–100 yr to guarantee the numerical stability. The injected energy has a Gaussian distribution around the explosion site with a width of 20 pc. Radiative cooling of the ISM is described by the term $\rho\Lambda$ in the energy equation, where the cooling function

$$\Lambda = \Lambda_i T^{\beta_i} \quad (8)$$

as derived by Dalgarno & McCray (1972) and Raymond, Cox and Smith (1976); Λ_i and β_i are given in Table 1.

In a SN explosion a fraction of the progenitor star mass is injected into the ISM. In our model the mass injection, which occurs simultaneously with the release of thermal energy, is described by the source term Π in the continuity equation,

$$\Pi = \frac{M_{\text{SN}}}{\rho V \Delta t}, \quad (9)$$

where M_{SN} is the injected mass, chosen to be $3M_\odot$. The mass of the interstellar gas within the volume (of a radius 10 pc) where the SN energy is released is about $10M_\odot$, so our results are hardly sensitive to the variation of M_{SN} if only it is less than $10M_\odot$.

Table 1. Parameters for the cooling function, Eq. (8).

T_i [K]	Λ_i [erg s ⁻¹ g ⁻² cm ³]	β_i
100	1.14×10^{15}	2.000
2000	5.08×10^{16}	1.500
8000	2.35×10^{11}	2.867
10^5	9.03×10^{28}	-0.650

2.2. The code

We assume periodic boundary conditions in the y direction, and sliding, periodic boundaries in the x direction. At the top and bottom boundaries we apply open boundary conditions with any inflow prohibited. This results in mass and energy loss through the top and bottom boundaries; in a typical simulation, about 10% of the total mass and energy escape from the box in 100 Myr.

Eqs. (2)–(5) are solved numerically using a third-order Hyman (1979) scheme for the time stepping and sixth-order compact scheme for the spatial derivatives (Lele 1992). We adopt artificial viscosities to capture shocks and hyper-viscous fluxes to stabilize advection and waves. The shock capturing viscosity is non-vanishing in the regions where $-\nabla \cdot \mathbf{u} > 0$ and proportional to $-\nabla \cdot \mathbf{u}$ there. The hyper-viscosity is proportional to the modulus of the ratio of the third to the first derivative of the velocity field. The diffusion coefficients $\nu = \eta = \chi$ mostly come from the artificial viscosities, the ordinary viscosities being negligible. The effective kinetic Reynolds number, based on the rms velocity and the scale of 150 pc, is approximately 300. A more detailed description of the numerical method is given in Brandenburg et al. (1995) and Nordlund & Stein (1990).

3. The initial state of the ISM

The initial state of the ISM for the SB runs discussed here is taken from our previous calculations, which model the hot and warm phases of the ISM with parameters corresponding to the solar neighborhood (Korpi et al. 1999). In these calculations the size of the computational domain is $0.5 \times 0.5 \times 2$ kpc in the radial, azimuthal and vertical directions, respectively and the corresponding mesh size is $63 \times 63 \times 254$. The Galactic symmetry plane, $z = 0$, is placed in the midplane of the computational domain. The box is located at a reference distance $R = 10$ kpc from the rotation axis and the centre of the box is rotating with angular velocity $25 \text{ km s}^{-1} \text{ kpc}^{-1}$ around the Galactic centre. We adopt a flat rotation curve, i.e. $\Omega \propto r^{-1}$, which yields the shear parameter $q = 1$.

SNe are introduced as instantaneous, localized explosive events each releasing thermal energy $E_{SN} = 10^{51}$ erg and the mass $3M_{\odot}$. We include both Type I and II SNe in our calculations. For Type II SNe we take the SN rate per unit area $\sigma_{II} = 3 \times 10^{-5} \text{ kpc}^{-2} \text{ yr}^{-1}$ corresponding to a frequency $1/44 \text{ yr}^{-1}$ in the whole Galaxy and for Type I, $\sigma_{I} = 4 \times 10^{-6} \text{ kpc}^{-2} \text{ yr}^{-1}$ corresponding to $1/330 \text{ yr}^{-1}$ (Tammann et al. 1994). In the vertical direction we assume an exponential distribution of the SN explosion rate per unit volume. The SN scale heights adopted

are 325 pc (Heiles 1987) and 90 pc (Miller & Scalo 1979) for Type I and II SNe, respectively. Type I SNe remain uncorrelated, whereas for Type II SNe we choose the explosion site randomly in the horizontal plane, but exclude those positions where the density is less than the average in that layer. Ferrière (1998) estimates that approximately 60% of Type II SNe are correlated, whereas Heiles (1987) gives the fraction 75% for clustered Type II SNe. With our prescription, 70% of Type II SNe remain correlated.

The system rapidly segregates into two phases, as can be seen from Fig. 1, where we plot probability density functions (PDFs) for density, temperature and total pressure taken at three different times (30, 60 and 80 Myr) of the simulation run. There is a warm phase, $T_w \simeq 10^4$ K and $n_w \simeq 0.1 \text{ cm}^{-3}$, most of which is concentrated near the Galactic midplane. In this region ($|z| \leq 0.25$ kpc, plotted with solid lines) the density (panels a, d and g) and temperature (panels b, e and h) PDFs have a well-pronounced double-peaked form. With increasing distance from the midplane the hot gas, $T_h \simeq 10^6$ K and $n_h \simeq 10^{-3} \text{ cm}^{-3}$, gradually becomes dominant; in the PDFs the peak corresponding to the hot phase becomes stronger (dashed and dotted lines). In the temperature PDFs the borderline between warm and hot phases occurs at a temperature $T = 10^5$ K, where the cooling function is maximum. The PDF of total pressure has a well-pronounced peak at about $1\text{--}2 \times 10^3 \text{ K cm}^{-3}$, the value common for all the phases which does not change significantly in time (compare panels c, f and i in Fig. 1), but varies with height. This indicates that the system has settled into a pressure equilibrium.

The volume filling factor of the hot gas is on average 30–40% after 15 Myr, during which SNe have stirred the whole volume. The filling factor grows with height from about 20–30% at the midplane to 80–100% at $|z| \approx 1$ kpc. The time-averaged scale height of the warm gas is 180–200 pc, which is close to that under hydrostatic equilibrium supported by thermal and turbulent pressures. Due to its large isothermal scale height, the hot gas is involved in a systematic vertical motion as it streams to the halo at a speed of $100\text{--}200 \text{ km s}^{-1}$, and is therefore far from hydrostatic equilibrium in our computational box. Nevertheless the horizontally averaged density of the hot component decreases with height at a scale of 600–700 pc.

There is also some cold dense gas, $T_c \simeq 10^3$ K and $n_c \simeq 1 \text{ cm}^{-3}$, arising from supernova compression. It can be distinguished in the density PDF as a wide wing at higher densities. The cold gas concentrates at $|z| \leq 100$ pc, and appears mainly in cloud-like structures in regions where many expanding SNe collide. It is not clear whether this gas can be described as a separate physical phase, because our model does not include self-gravity or thermal instability, or any other physical effect that would be supporting this phase.

For orientation, at the initial state of the SB runs (60 Myr), the scale height of the density distribution is $H \approx 180$ pc, the average density at the midplane is $n_0 \approx 1.1 \text{ cm}^{-3}$, thermal pressure $p \approx 2 \times 10^{-12} \text{ dyn cm}^{-2}$, turbulent pressure $p_t \approx 3 \times 10^{-13} \text{ dyn cm}^{-2}$ and magnetic pressure $p_m \approx 5 \times 10^{-14} \text{ dyn cm}^{-2}$ at the midplane. Using Eq. (1), this yields $D \approx 50$ for a SB of a luminosity $3 \times 10^{37} \text{ ergs}^{-1}$ in the ini-

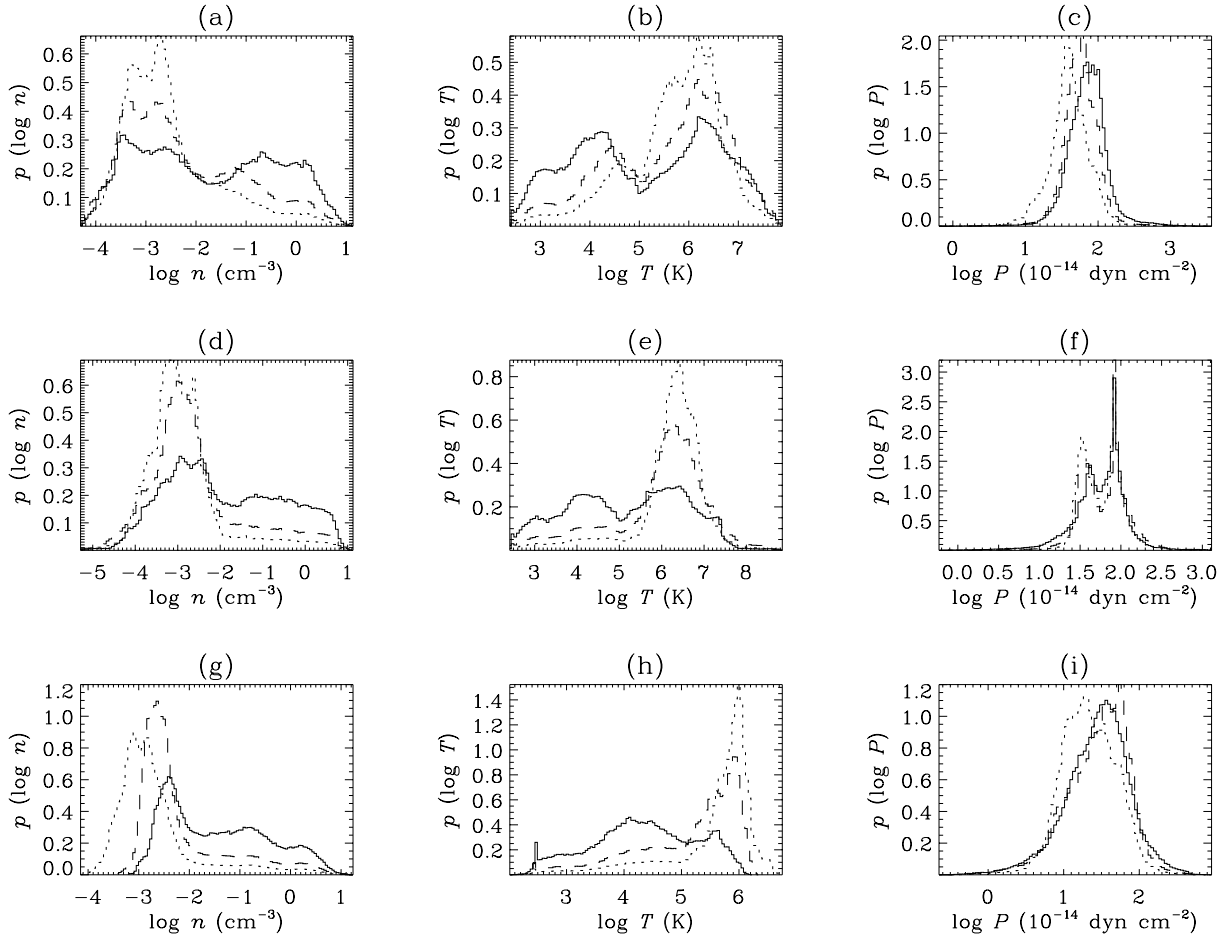


Fig. 1a–i. Probability density functions for logarithms of density (panels **a**, **d** and **g**), temperature (panels **b**, **e** and **h**) and total pressure (panels **c**, **f** and **i**) at 30 Myr (upper row), 60 Myr (middle row) and 80 Myr (lower row) of the simulation. PDFs calculated over the whole computational volume for $|z| < 0.25$ kpc, $|z| < 0.5$ kpc and $|z| < 1$ kpc are plotted with solid, dashed and dotted lines, respectively. The initial ISM for the SB run is taken at 60 Myr of this simulation run.

tial ISM; according to the criterion of Mac Low and McCray (1988), a typical SB would not blow out of the disc with these parameters.

The system is fed by the thermal energy injected in SN explosions, which is converted to kinetic energy of expansion during the early stages of SN evolution. The SN energy is further transformed to turbulent energy at later stages, when the remnants become deformed by their inhomogeneous surroundings. The velocity field in our simulations resembles fully developed turbulence. Although the forcing provided by SNe is of a compressible nature, 60–90% of the total turbulent energy is in vortical motions. The efficient generation of vorticity occurs partly because expanding SNRs rapidly lose their spherical symmetry due to the density inhomogeneities in the surrounding medium. Other active vorticity generation mechanisms are the baroclinic effect, and the stretching of vortex lines (Korpi et al. 1998; cf. Bykov & Toptygin 1987). Those rare remnants that occur in dense homogeneous regions and so remain spherical throughout their lifetime contribute to the longitudinal compressible motions in the ISM.

Statistical parameters of turbulence are significantly different in different phases of the ISM (Korpi et al. 1999). The r.m.s. total velocity (with any systematic component subtracted) remains fairly constant with height being $v_w \approx 10 \text{ km s}^{-1}$ and $v_h \approx 40 \text{ km s}^{-1}$ for the warm and hot components, respectively. These values are in good agreement with observational estimates of turbulent velocities at small heights and in the Reynolds layer (Kulkarni & Fich 1985; Reynolds 1985, 1991; Wang et al. 1997). Whereas v_w is close to the speed of sound at temperature 2×10^4 K, v_h is significantly smaller than the speed of sound at temperature 10^6 K. The hot gas, however, has a systematic upward motion with velocities $100\text{--}200 \text{ km s}^{-1}$. This kinetic energy can be transformed into disordered, turbulent motions, resulting in higher turbulent velocities in the halo. Kalberla et al. (1998) report random motions with r.m.s. velocity 60 km s^{-1} in the Galactic halo.

The correlation scale in the warm phase is $l_w \approx 30$ pc and does not vary much with height. This indicates a well-mixed turbulent layer with turbulent cells of ≈ 60 pc in size. The correlation scale of the hot gas increases with height from $l_h \approx 20$ pc at the midplane to $l_h \approx 60$ pc at $z = 150$ pc. This correlation

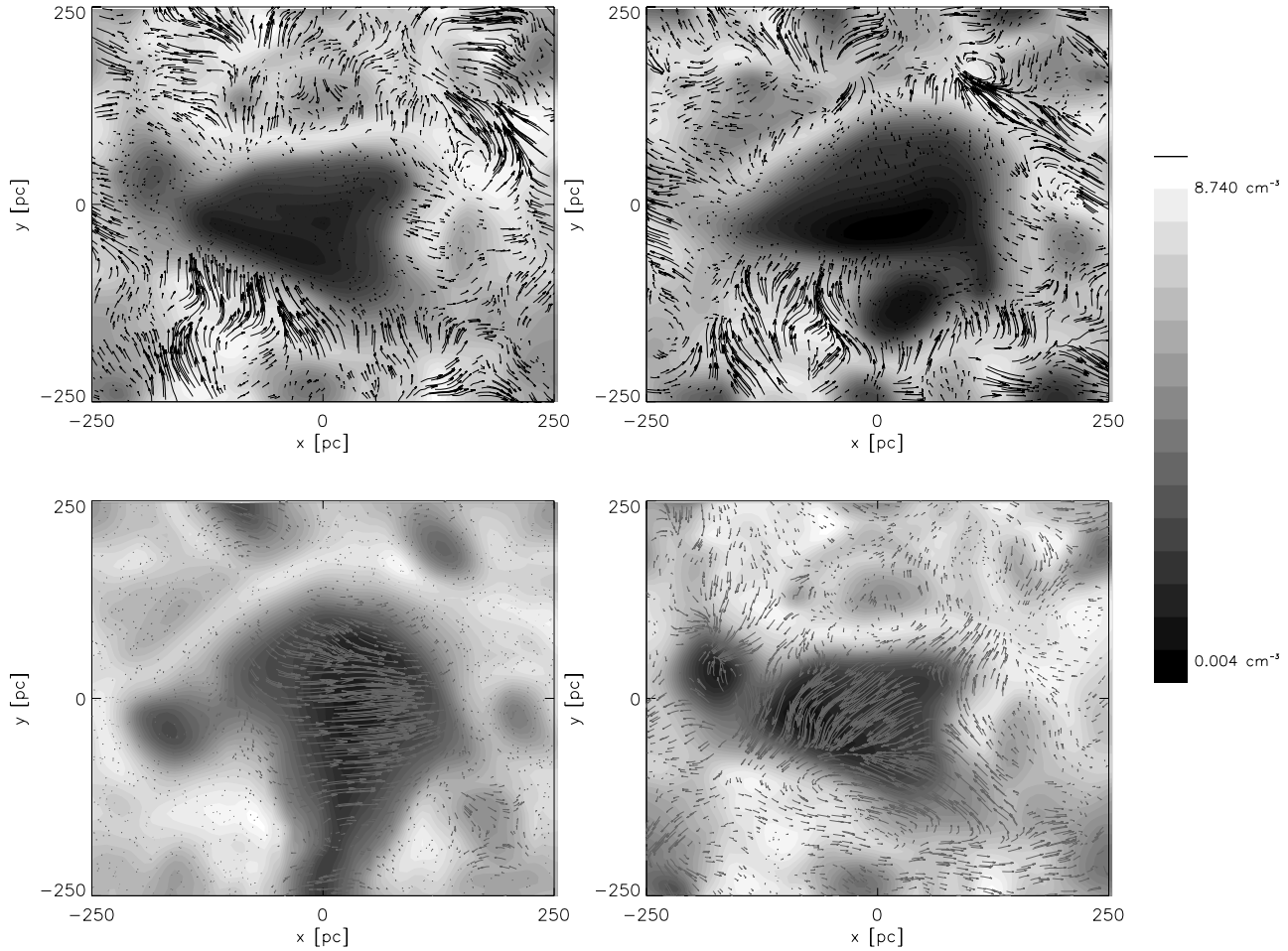


Fig. 2. Horizontal slices at the midplane ($z = 0$) at four different times of the SB calculation (90, 95, 100 and 105 Myr from left to right and from top to bottom). The shades of grey show the logarithm of gas density, the grey arrows the velocity field (lower row) and the black arrows the magnetic field (upper row). The length of the arrows indicates the strength of the fields; the maximum field strength corresponding to the longest arrow is $1\mu\text{G}$ in the upper row and 1500km s^{-1} in the lower row.

scale hardly characterizes turbulence in the hot component, but rather reflects a typical size of a region occupied by the hot gas, which grows with z together with the filling factor of the hot gas.

At the initial state of these calculations, $t = 0$, we apply a uniform, azimuthally directed magnetic field of the strength $0.1\mu\text{G}$, which is rapidly amplified to $1.3\mu\text{G}$ strength. At $t = 60$ Myr, the magnetic field has an average component of a strength $0.5\mu\text{G}$ and a random component which is approximately 1.5 times stronger than the mean. The magnetic field has an approximately Gaussian vertical distribution with a scale height 200 pc. The anticipated time scale of the evolution of the mean Galactic magnetic field is several hundred Myr (see, e.g., Beck et al. 1996), so the magnetic field in our simulations can hardly represent a steady state.

4. Evolution of a superbubble

We follow the evolution of a SB introduced at the centre of the computational domain ($x = y = z = 0$) at a time $t = 60$ Myr

in the calculation described in the previous section, which time is also the starting time of the SB calculation. The SB is initiated by SNe exploding in a small region of $3 \times 3 \times 3$ grid points (about $23 \times 23 \times 23\text{pc}$) around the centre. The SB parameters are typical in the Galaxy (e.g. Heiles 1987): the SN frequency within the SB is taken as in an OB association, $f_{\text{SN(OB)}} = 10^{-6}\text{yr}^{-1}$; the lifetime of the association is $5 \times 10^7\text{yr}$; the resulting SB luminosity is $3 \times 10^{37}\text{ergs}^{-1}$. Other SN activity continues in the medium outside the SB, where Type II SNe now have a frequency $f_{\text{SNII}} = f - f_{\text{SN(OB)}}$. Here f is the total frequency corresponding to σ_{II} discussed in the Sect. 3. The SNe not only provide a realistic heating of the SB environment, but also maintain an appropriate degree of nonuniformity, multiphase structure and magnetic field in the simulated ISM.

The SB evolves in an environment which has a regular *average* vertical density stratification, but the density field has strong local variations in all directions due to the background SN activity. Because Type II SNe have a smaller scale height, they mostly occur near the midplane where the average density is large. Therefore Type II SNe, if isolated, produce small

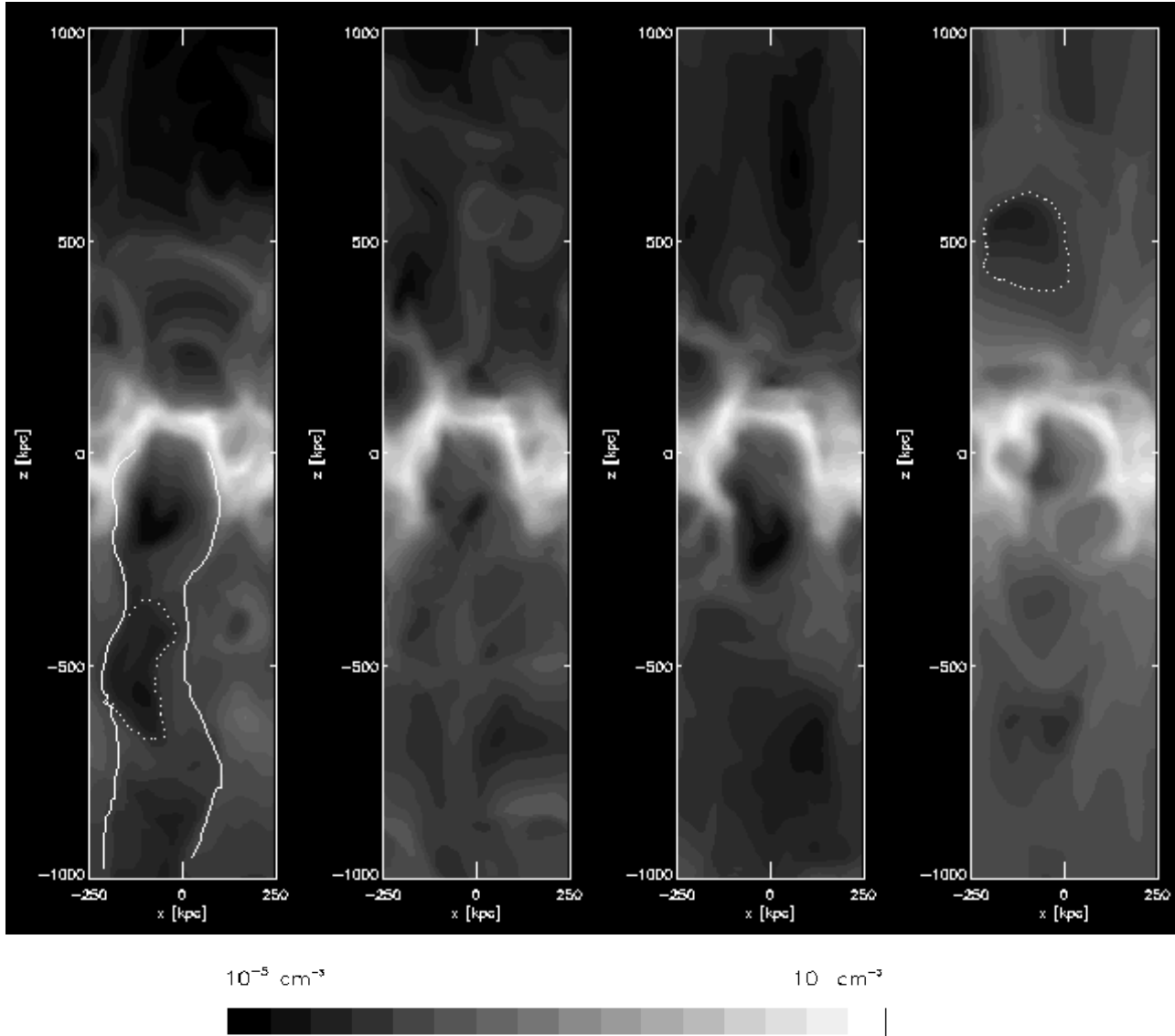


Fig. 3. Slices of the logarithmic density field in the xz -plane starting at 93 Myr, with 1.5 Myr interval. A SB has formed in the middle of the box ($x = 0$, $y = 0$, $z = 0$), and evolved for 33 Myr. In the upper disk plane the SB has remained rather spherical, but in the lower plane it has been able to break through the disk; a chimney-type structure is seen at 93 Myr (leftmost panel). Due to Type I SNe, which explode at higher altitudes, matter is pushed downwards, and the superbubble becomes confined again at 97 Myr.

remnants with a typical size of 50 pc at the midplane; many of them can be seen in Fig. 2, where we show horizontal slices of the density distribution at four different times. As can be seen in Fig. 2, Type II SNe produce a complicated network of warm gas which confines hot, dilute gas in the form of tunnels and cavities. Approximately 70% of Type II SNe occurring outside the SB are clustered in our model, and therefore they can produce superstructures by themselves. One such structure can be seen in the upper right panel in Fig. 2 (at about $x = 0$, $y = -150$ pc); later on this bubble merges with the SB (see lower left panel).

A SB does not remain spherical in this nonuniform environment. It is an irregular cavity of a size about 200 pc filled with hot gas and surrounded by a warm shell. The bubble changes its shape dynamically due to the continuous mixing of the gas

in the computational domain; the bubble can even shrink in size (compare the lower left and right panels in Fig. 2) during epochs of high SN compression in the surrounding medium. Inside the SB, filled with hot, low-density gas, expansion velocities of SNe are very high, of the order of 1000 km s^{-1} ; this can be seen in the lower panels of Fig. 2. Magnetic field is expelled from the SB interior and becomes confined to the warm shell (see upper panels in Fig. 2).

Isolated Type I SNe have a larger scale height, and therefore they frequently occur in the low-density gas, including that at large heights, producing large bubbles (150–200 pc in size) of hot gas; see for example the rightmost panel in Fig. 3, where one of them is visible approximately at the height of about 500 pc (marked with dotted line). The role of Type I SNe for the SB evo-

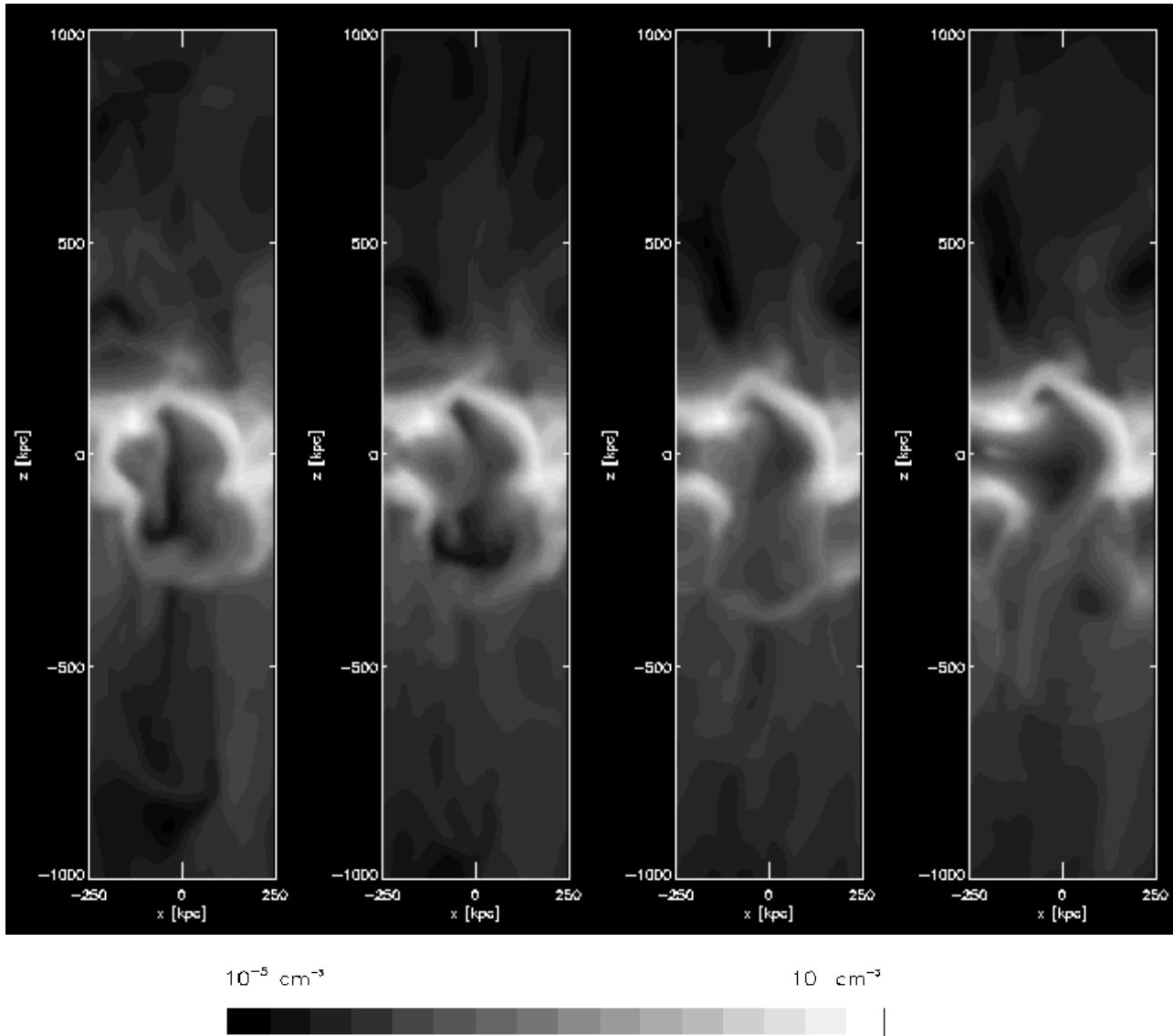


Fig. 4. Same as Fig. 3, but starting at 97 Myr with 0.5 Myr interval. The superbubble is an irregular cavity confined to the disk, and remains that way for approximately 3 Myr.

lution is twofold. Due to the average density stratification, the SB expands more rapidly in the direction of decreasing density (upwards or downwards in the upper and lower parts of the disk, respectively). When it meets a cavity caused by a Type I SN, it can easily accelerate and produce a chimney-type structure. On the other hand, newly exploded Type I SNe can effectively prevent the expansion of a SB, because, in addition to transporting matter away from the disk, some mass is also pushed towards it. When the SB collides with a Type I SN shell moving towards the disk, the SB becomes decelerated.

The SB evolves in a very dynamic manner in the vertical direction also. After approximately 30 Myr of evolution, it has broken through the lower disk plane, and produced a chimney-type structure, which can be seen in the leftmost panel of Fig. 3 (marked with solid line). The break-through was facilitated by a Type I SN that exploded at the height of 500 pc just below the SB

(marked with dotted line). Within the next few Myr the chimney is destroyed by the surrounding SN activity. The SB becomes an irregular cavity confined in the disk, and remains that way for the next 3 Myr (see Figs. 3 and 4). After 40 Myr of evolution the SB starts to expand rapidly both upwards and downwards from the disk (leftmost panel in Fig. 5). It is able to break through as a chimney-type structure in the upper part of the computational domain, but in the lower part the break-through is prevented by another superstructure, which itself seems to form a chimney.

In Fig. 6 we show the density, velocity and magnetic field slightly before (102 Myr) and after (104 Myr) the chimney has formed. At 102 Myr expanding bubbles elongated in the vertical direction are observed on both sides of the disk. The magnetic field is strong and vertically directed at the foot-points of these bubbles. The expanding shells are also magnetized, and at the top the magnetic field tends to be directed parallel to the disk. At

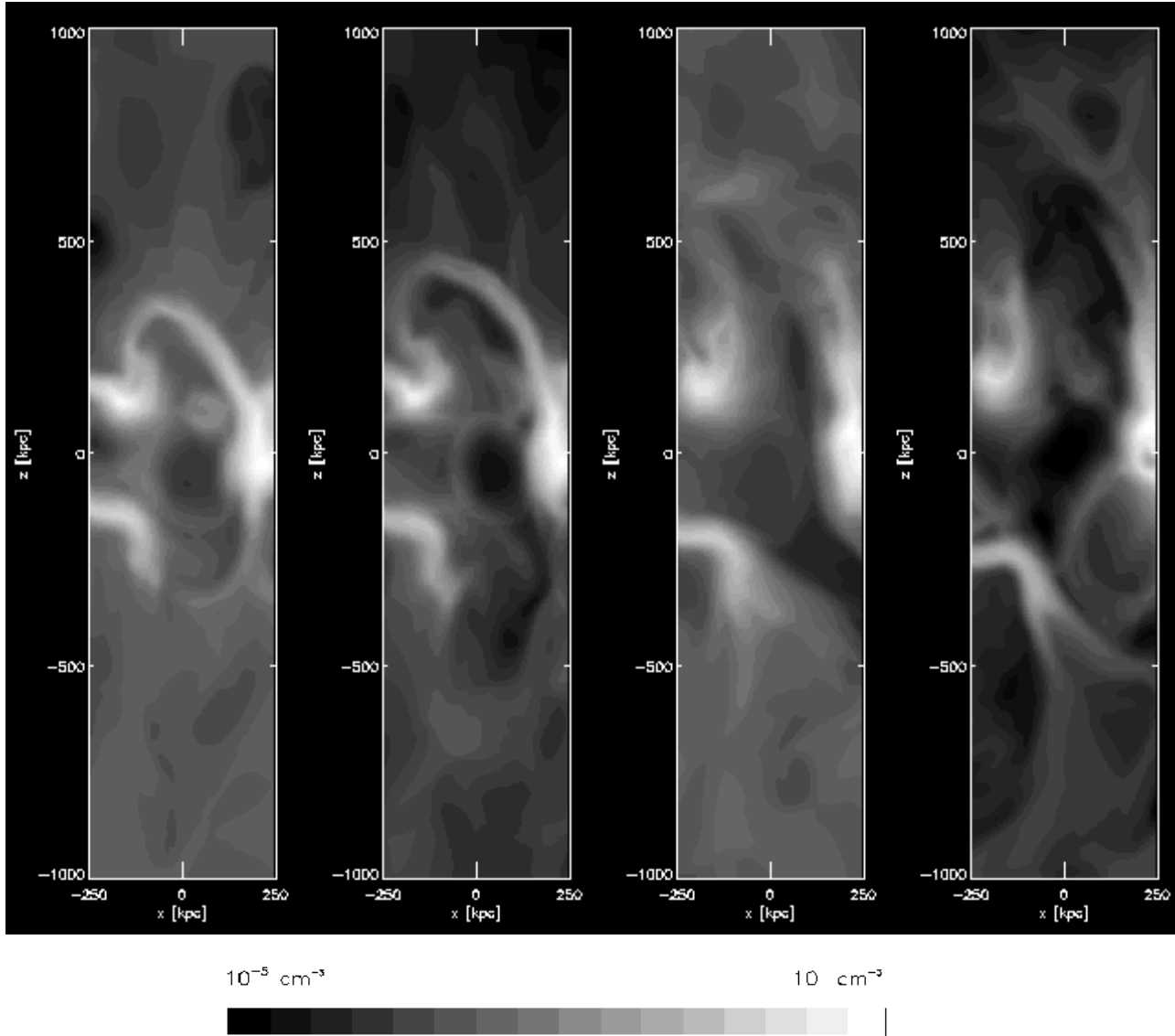


Fig. 5. Same as Fig 3 and 4, but starting at 100 Myr with 1.5 Myr interval. The SB has started to accelerate both downwards and upwards. It blows out in the upper part, but in the lower part the blow-out is prohibited by another SN cluster.

104 Myr the bubble in the upper part has formed a chimney: the bubble is open at the top, and the flow of hot matter is directed slightly leftwards because of a Type I SN exploded nearby. The break-through of the bubble in the lower part was prevented by another superstructure: a strong vertical magnetic field is observed at the interface of the superstructures.

5. Conclusions

We have followed the evolution of a SB with a luminosity typical for the SBs in the Galaxy, in a multi-phase, turbulent and magnetized ISM regulated by SNe. The SB evolves in a dynamic manner: it is an irregular cavity of the size 200 pc, filled with hot gas and surrounded by a warm, magnetized shell, which quickly changes its shape as the simulated ISM is mixed by SNe. During its lifetime (5×10^7 yr) the SB can go through several chimney-phases, between which it becomes confined to the

disk. These results indicate that a SB, which would not be able to break through a homogeneous stratified disk, can produce chimney-type structures, persisting over a few Myr, in a turbulent, inhomogeneous medium. The lifetime of these structures, however, is always shorter than 10^7 yr.

Acknowledgements. This work was supported by the EC Human Capital and Mobility Networks project No. CHRX-CT-0483 (M. J. K. and I. T.) and PPARC grant PPA/G/S/1997/00284.

References

- Beck R., Brandenburg A., Moss D., Shukurov A., Sokoloff D., 1996, ARA&A 34, 155
- Brandenburg A., Nordlund Å., Stein R.F., Torkelsson U., 1995, ApJ 446, 741
- Bykov A.M., Toptygin I.N., 1987, Ap&SS 138, 341
- Dalgarno A., McCray R.A., 1972, ARA&A 10, 375

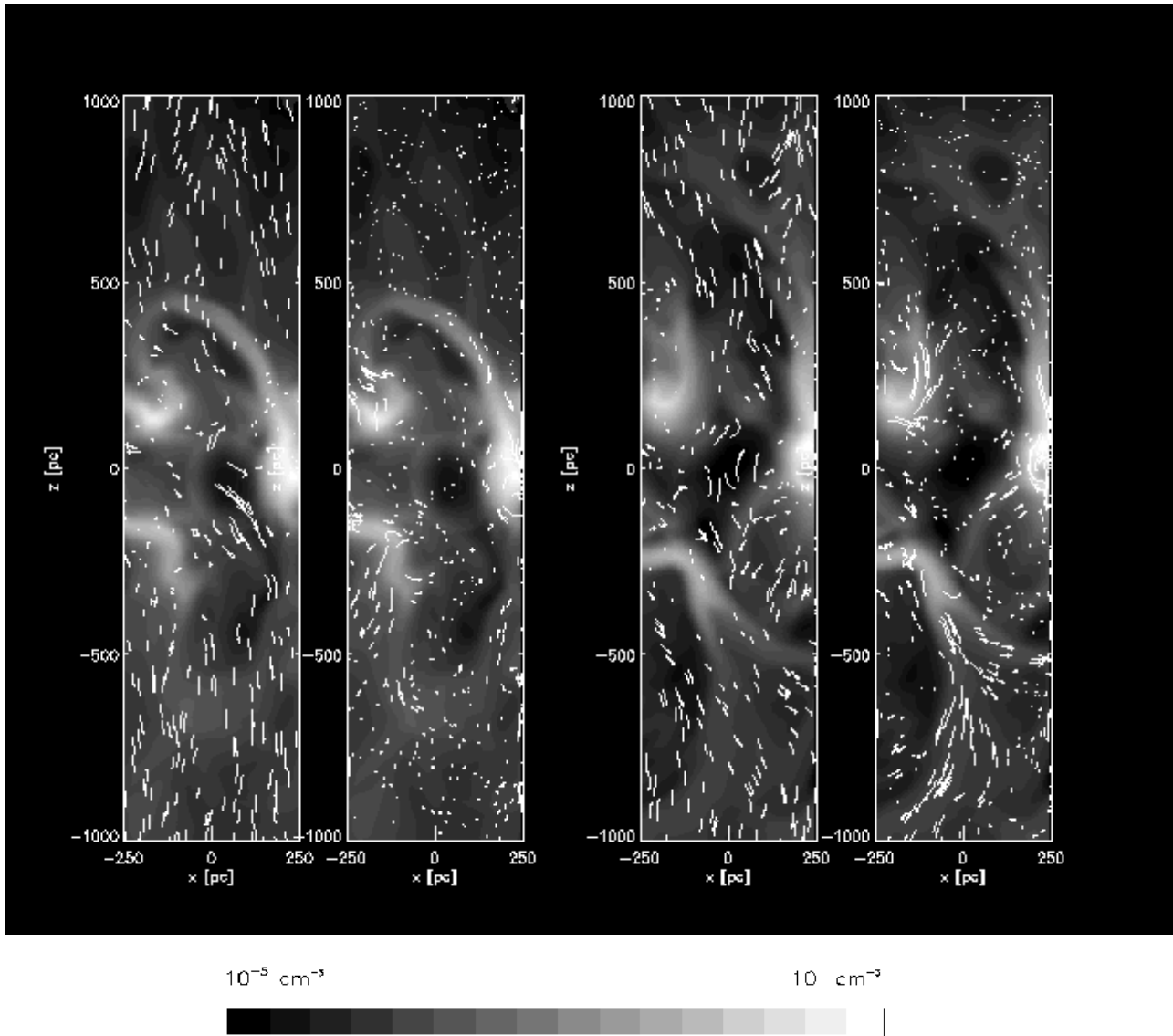


Fig. 6. Density, velocity and magnetic field slightly before (102 Myr; the two panels on the left) and after (104 Myr; the two panels on the right) a chimney has formed in the upper part of the computational domain. In the first and third panel from the left the arrows represent the velocity field vector projections in the plane of the sky, and in the second and fourth panel magnetic field vectors are plotted.

Ferrière K., 1998, *ApJ* 497, 759

Ferrière K.M., Mac Low M.-M., Zweibel E.G., 1991, *ApJ* 375, 239

Heiles C., 1984, *ApJS* 55, 585

Heiles C., 1987, *ApJ* 315, 555

Heiles C., 1990, *ApJ* 354, 483

Hyman J.M., 1979, In: Vecnevetsky R., Stepleman R.S. (eds.) *Adv. Computation Methods for Partial Differential Equations Vol. III*, Publ. IMACS, p. 313

Kalberla P.M.W., Westphalen G., Mebold U., Hartmann D., Burton W.B., 1998, *A&A* 332, L61

Koo B.-C., McKee C.F., 1992, *ApJ* 388, 93

Koo B.-C., Heiles C., Reach W.T., 1992, *ApJ* 390, 108

Korpi M.J., Brandenburg A., Shukurov A., Tuominen I., 1998, In: Franco J., Carraminana A. (eds.) *Interstellar Turbulence. Proc. 2nd Guillermo Haro Conference*, Cambridge University Press, p. 16

Korpi M.J., Brandenburg A., Shukurov A., Tuominen I., Nordlund Å., 1999, *ApJ* 514, L99

Kuijken K., Gilmore G., 1989, *MNRAS* 239, 605

Kulkarni S.R., Fich M., 1985, *ApJ* 289, 792

Lele S.K., 1992, *J. Comput. Phys.* 103, 16

Lockman F.J., 1984, *ApJ* 283, 90

Mac Low M.-M., McCray R., 1988, *ApJ* 324, 776

Mac Low M.-M., McCray R., Norman M.L., 1989, *ApJ* 337, 141

McCray R., Kafatos M., 1987, *ApJ* 317, 190

Miller G.E., Scalo J.M., 1979, *ApJS* 41, 513

Nordlund Å., Stein R.F., 1990, *Comput. Phys. Comm.* 59, 119

Norman C.A., Ikeuchi S., 1989, *ApJ* 345, 372

Normandeau M., Taylor A.R., Dewdney P.E., 1996, *Nat* 380, 687

Raymond J.C., Cox D.P., Smith B.W., 1976, *ApJ* 204, 290

Reynolds R.J., 1985, *ApJ* 294, 256

Reynolds R.J., 1991, In: Bloemen H. (ed.) *Proc IAU Symp. 144, The Interstellar Disk-Halo Connection in Galaxies*. Kluwer, Dordrecht, p. 67

Slavin J.D., Cox D.P., 1993, *ApJ* 417, 187

- Spitzer L. Jr., 1990, ARA&A 28, 71
Tammann G.A., Löffler W., Schröder A., 1994, ApJ 92, 487
Tenorio-Tagle G., Bodenheimer P., 1988, ARA&A 26, 145
Tenorio-Tagle G., Rozyczka M., Bodenheimer P., 1990, A&A 237, 207
Tomisaka K., 1990, ApJ 361, L5
Tomisaka K., 1998, MNRAS 298, 797
Tomisaka K., Ikeuchi S., 1986, PASJ 38, 697
Wang J., Heckman T.M., Lehnert M.D., 1997, ApJ 491, 114
Wisdom J., Tremaine S. 1988, AJ 95, 925